*Computational Modelling of Concrete and Concrete Structures – Meschke, Pichler & Rots (Eds)*


# Modelling of cracking mechanisms in cementitious materials: The transition from diffuse microcracking to localized macrocracking

I.C. Mihai & A. Bains
*Cardiff University, Cardiff, UK*

P. Grassl
*Glasgow University, Glasgow, UK*

ABSTRACT: Cracking in cementitious materials still poses significant and interesting modelling challenges and structural designers need reliable tools for an accurate prediction of crack widths. The paper presents a numerical study into cracking mechanisms in cement based materials using lattice simulations employing the model of Grassl & Antonelli (2019). Furthermore, a micromechanics based constitutive model is proposed that focuses on representing the transition from diffuse microcracking to localized macrocracking. The model includes an Eshelby based two-phase composite solution to represent the aggregate particles embedded in a cementitious matrix, directional microcracking and a criteria for the transition from diffuse microcracking to localised macrocracking. By removing the macrocrack fracture strain component from the strain which drives microcrack growth, the effect of macrocrack development on microcrack growth in various other directions is included. Numerical simulations show that the model captures well the mechanical behaviour as well as key characteristics of the cracking mechanism in cementitious materials.

## 1 INTRODUCTION

Microcracks are present in concrete before loading is applied and are concentrated at the interfacial transition zone (ITZ) between the cementitious matrix and aggregate particles (Slate& Hover 1984). If an applied tensile load is increased past the initiation threshold, the microcracks propagate and further microcracks are progressively initiated in the ITZ of smaller aggregate particles (Karihaloo 1995). As the load increases further, some microcracks will grow and coalesce to form a macrocrack (Jenq & Shah 1991). For both uniaxial tension and uniaxial compressive loading, these macrocracks tend to form around the peak load and propagate unstably with the material around the zone of macrocracking unloading (Shah et al. 1995; Vonk 1992; i.e., cracking becomes concentrated within a certain zone. The process of cracking becoming concentrated to macrocracks formed by the coalescence of diffuse microcracks is often referred to as crack localisation.

This paper presents the main details of a micromechanics based constitutive model for cementitious materials that simulates crack localization. A series of numerical experiments employing a lattice model were carried out to study the transition from discrete microcracking to localized macrocracking and the results from these studies were used guide the development of the constitutive model.

## 2 CRACK LOCALIZATION STUDY

### 2.1 *Lattice model*

A study into the transition from diffuse microcracking to localized macrocracking was carried out with the lattice model of Grassl & Antonelli (2019) which relies on periodic meso-structure generation by employing a representative cell with a periodic lattice network and periodic boundary conditions. Within the computational cell, the meso-structure of concrete was modelled considering three material phases; namely the mortar matrix, the coarse aggregate particles and the ITZ respectively (Figure 1). The aggregate particles are idealized as ellipsoids, the size distribution of which is determined based on Fuller's grading curve.

### 2.2 *Constitutive relationships for the lattice model*

For this study, the aggregate particles are assumed to have a linear elastic behaviour and the scalar damage relationship in Equation 1 is employed to simulate the mechanical behaviour of both the matrix and the ITZ.

$$\boldsymbol{\sigma} = (1 - \omega_a)\, \mathbf{D}_e \boldsymbol{\varepsilon} \tag{1}$$

where $\boldsymbol{\sigma}$ is the stress vector, $\boldsymbol{\varepsilon}$ is the strain vector, $\mathbf{D}_e$ is the elastic stiffness matrix and $\omega_a$ is a scalar


DOI 10.1201/9781003316404-26

damage variable which is 0 at no damage and gradually increases to 1 for complete damage. The damage evolution is given in Equation 2:

$$(1-\omega_a)\,E\kappa_d = f_t e^{\left(-\frac{\omega_a h \kappa_d}{w_f}\right)} \quad (2)$$

where $E$ is the Young's modulus, $f_t$ is the tensile strength, $w_f$ is a parameter that controls the slope of the softening curve and is related to the fracture energy $G_f$ as follows; $w_f = G_f/f_t$. $\kappa_d$ is an equivalent strain parameter gouverned by a damage surface based on an ellipsoidal strength envelope in the stress space and standard loading/unloading conditions (Grassl & Bolander 2016).

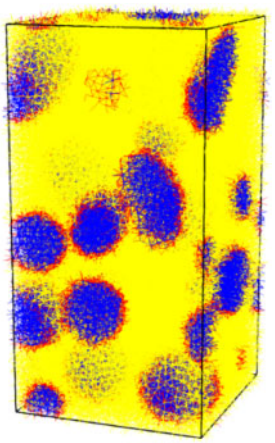

Figure 1. Representative computational cell showing the material phases; mortar matrix (yellow), corase aggregate particles (blue) and the ITZ (red).

### 2.3 *Crack localization*

A series of lattice simulations using the formulation described above were carried out, employing a $50 \times 50 \times 100$ (mm) periodic cell and the material parameters given in Table 1. Moreover, following a series of convergence studies, a lattice element size of 1.6 mm and aggregate particle diameters ranging from 10 mm to 20 mm were selected respectively.

Table 1. Material parameters - lattice simulations.

| | |
|---|---|
| $E_m$(MPa) | 30 000 |
| $E_{ITZ}$(MPa) | 45 000 |
| $E_\Omega$(MPa) | 90 000 |
| $f_{t,m}$ (MPa) | 3 |
| $f_{t,ITZ}$(MPa) | 1.5 |
| $G_{f,m}$ (J/m$^2$) | 120 |
| $G_{f,ITZ}$(J/m$^2$) | 60 |
| Volume fraction of aggregate, | $V_\Omega$40% |

A typical stress-relative displacement curve from a uniaxial tension simulation is presented in Figure 2 and associated crack patterns at different stages are presented in Figure 3, noting that only the active, growing cracks are shown at each stage.

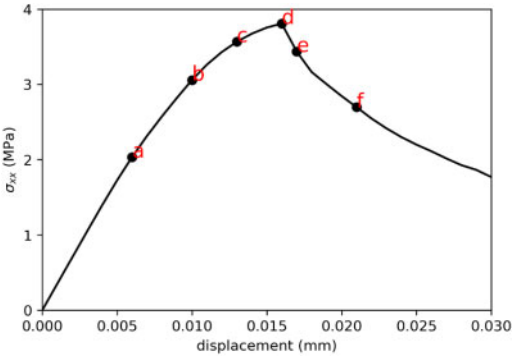


Figure 2. Stress-relative displacement curve from lattice model simulation of uniaxial tension (tension +ve).

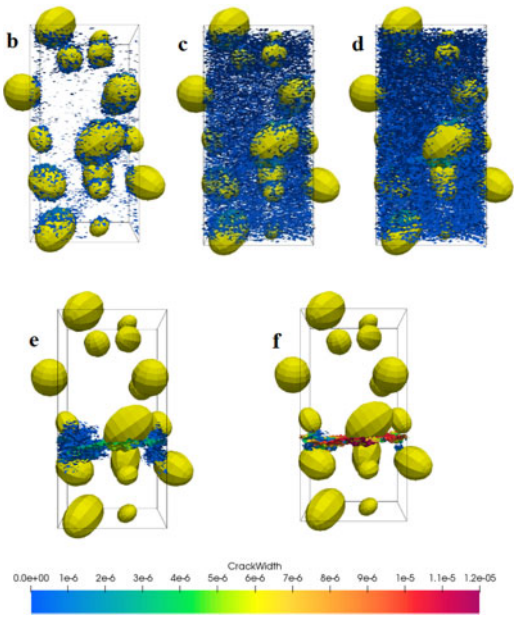


Figure 3. Crack patterns at different stages of damage. The different stages b - f correspond to those marked in Figure 2.

The crack patterns in Figure 3 show a number of cracking mechanisms, captured well by the lattice model. Microcracks are initiated at the matrix-aggregate interface and subsequently propagate in the cementitious matrix to a state of diffuse microcracking associated with pre-peak non-linearity (stages b-d). By contrast, the post-peak response is characterized by a single localized macrocrack (stages e-f).

The representation of these two distinct cracking stages and the transition from diffuse microcracking to

localized macrocracking is the focus of the constitutive model presented in Section 3.

## 3 MICROMECHANICS BASED CONSTITUTIVE MODEL

### 3.1 *Model concepts*

The constitutive model presented here aims to represent the behaviour at two stages of cracking; (i) the diffuse microcracking stage characteristic of the pre-peak behavior in tension and (ii) the localized macrocrack stage, characteristic of the post-peak behaviour respectively.

In the elastic state, before any damage occurs, the concrete material is modelled as a two-phase composite comprising a matrix representing the mortar and spherical inclusion representing the coarse aggregate particles. The diffuse microcracking stage is represented using a directional microcracking formulation based on the Budiansky & O'Connell (1976) solution. The localised macrocrack stage is then represented by removing a macrocrack fracture strain component from the strain which drives microcrack growth.

### 3.2 *Two-phase composite*

The elastic constitutive relationship for the two-phase composite is obtained by making use of the micromechanics Eshelby matrix-inclusion solution and the Mori-Tanaka homogenisation scheme (Mura, 1987) for a non-dilute distribution of inclusions:

$$\bar{\boldsymbol{\sigma}} = \mathbf{D}_{\mathrm{m}\Omega} : \bar{\boldsymbol{\varepsilon}} \tag{3}$$

where $\bar{\boldsymbol{\sigma}}$ and $\bar{\boldsymbol{\varepsilon}}$ are the average far-field stress and strain respectively. $\mathbf{D}_{\mathrm{m}\Omega}$ is the elasticity tensor of the composite:

$$\mathbf{D}_{\mathrm{m}\Omega} = (\mathrm{f_m}\mathbf{D}_{\mathrm{m}} + \mathrm{f}_\Omega \mathbf{D}_\Omega \cdot \mathbf{T}_\Omega) \cdot \left(\mathrm{f_m}\mathbf{I}^{4\mathrm{s}} + \mathrm{f}_\Omega \mathbf{T}_\Omega\right)^{-1} \tag{4}$$

in which $\mathbf{D}_\beta$ represents the elasticity tensor and $\mathrm{f}_\beta$ the volume fraction of $\beta$-phase ($\beta = \mathrm{m}$ or $\Omega$), $\mathrm{f_m} + \mathrm{f}_\Omega = 1$. $\mathbf{I}^{4s}$ is the fourth order identity tensor and

$$\mathbf{T}_\Omega = \mathbf{I}^{4s} + \mathbf{S}_\Omega \cdot [(\mathbf{D}_\Omega - \mathbf{D}_{\mathrm{m}}) \cdot \mathbf{S}_\Omega + \mathbf{D}_{\mathrm{m}}]^{-1} \cdot (\mathbf{D}_{\mathrm{m}} - \mathbf{D}_\Omega) \tag{5}$$

$\mathbf{S}_\Omega$ is the Eshelby tensor for spherical inclusions (Nemat-Nasser & Hori, 1993).

### 3.3 *Directional microcracking*

A solution based on the work of Budiansky & O'Connell (1976) is employed to address microcracking by evaluating the added strain $\boldsymbol{\varepsilon}_a$ from series of penny-shaped microcracks of various orientations distributed according to a crack density function $f(\theta, \psi)$. The added strains resulting from the microcracks are superimposed on the composite such that the constitutive relationship in Equation 3 becomes:

$$\bar{\boldsymbol{\sigma}} = \mathbf{D}_{\mathrm{m}\Omega} : (\bar{\boldsymbol{\varepsilon}} - \boldsymbol{\varepsilon}_{\mathrm{a}}) \tag{6}$$

The added strain are as follows (Budiansky & O'Connell, 1976):

$$\boldsymbol{\varepsilon}_{\mathrm{a}} = \left( \frac{1}{2\pi} \int_{2\pi} \int_{\pi/2} \mathbf{N}_\varepsilon : \mathbf{C}_a : \mathbf{N} f(\theta, \psi) sin(\psi) d\psi \mathrm{d}\theta \right) : \bar{\boldsymbol{\sigma}} \tag{7}$$

in which $\mathbf{C}_a$ is the local compliance tensor in the local coordinate system of a microcrack (**r**,**s**,**t**) and **N** the stress transformation tensor. In each direction, defined by ($\theta$, $\psi$), the crack density parameter is related to a directional scalar damage parameter $\omega$ ($0 \leq \omega \leq 1$) such that:

$$f(\theta, \psi)\mathbf{C}_a = \frac{\omega(\theta, \psi)}{1 - \omega(\theta, \psi)} \mathbf{C}_{\mathrm{L}} = \mathbf{C}_\alpha(\theta, \psi) \tag{8}$$

where $\mathbf{C}_{\mathrm{L}} = \frac{1}{E_m} \begin{bmatrix} 1 & 0 & 0 \\ 0 & \frac{4}{2 - \nu_m} & 0 \\ 0 & 0 & \frac{4}{2 - \nu_m} \end{bmatrix}$ is the local elastic compliance tensor, with $\nu_m$ and $E_m$ being Poisson's ratio and Young's modulus of the matrix phase respectively.

The local damage function from Mihai & Jefferson (2011) is employed to govern the evolution of the damage parameter $\omega$ and is given by:

$$F_\zeta(\boldsymbol{\varepsilon}_L, \zeta) = \left( \varepsilon_{Lrr} \frac{1 + \alpha_L}{2} + \sqrt{\varepsilon_{Lrr}^2 \left( \frac{1 - \alpha_L}{2} \right)^2 + r_L^2 \left( \varepsilon_{Lrs}^2 + \varepsilon_{Lrt}^2 \right)} \right) - \zeta \tag{9}$$

in which $\alpha_L = \frac{\nu_{\mathrm{m}}}{1 - \nu_{\mathrm{m}}}$, $\mathrm{r}_L = \frac{\nu_{\mathrm{m}} - 1/2}{\nu_{\mathrm{m}} - 1}$ and noting that the following loading/unloading conditions apply:

$$F_\zeta \leq 0;\ \dot{\zeta} \geq 0;\ F_\zeta \dot{\zeta} = 0 \tag{10}$$

Introducing Equation 7 and Equation 8 into Equation 6 and rearranging gives:

$$\bar{\boldsymbol{\sigma}} = \mathbf{D}_{mc} : \bar{\boldsymbol{\varepsilon}} \tag{11}$$

where;

$$\mathbf{D}_{\mathrm{mc}} = \left( \mathbf{I}^{4\mathrm{s}} + \frac{\mathbf{D}_{\mathrm{m}\Omega}}{2\pi} \int_{2\pi} \int_{\frac{\pi}{2}} \mathbf{N}_\varepsilon : \mathbf{C}_\alpha(\theta, \psi) : \times \mathbf{N} \cdot \sin(\psi) d\psi d\theta \right)^{-1} \cdot \mathbf{D}_{\mathrm{m}\Omega} \tag{12}$$

### 3.4 *Macrocracking*

The model assumes that macrocracks form when the overall stress reaches its peak value i.e.:

$$\frac{d\sigma_I}{d\varepsilon_I} = \mathbf{0} \tag{13}$$

where $\sigma_I$ and $\varepsilon_I$ are the major principal stress and strain respectively. Under tensile loading, the normal directions of macrocrack plane are based on the orientations of the major principal strains and a maximum of two macrocracks are allowed to form. Under compressive loading, a macrocrack forms with the normal to the crack plane given by the direction which maximises the effective strain parameter at the peak stress.

Macrocrack formation is taken into account in the overall constitutive relationship by removing the macrocrack inelastic strain from the average strain:

$$\bar{\mathrm{s}} = \mathbf{D}_{mc} : \left( \bar{+} - \sum_{i=1}^{n_{sd}} \mathbf{N}_{\varepsilon}(\alpha_i, \beta_i) : \hat{\boldsymbol{\varepsilon}}_i \right) \tag{14}$$

where $n_{sd}$ is the total number of macrocrack planes and $\hat{\boldsymbol{\varepsilon}}$ is the macrocrack inelastic strain. $\alpha$and $\beta$ are the orientation angles of the macrocrack plane. The local stress of macrocrack planes $\tilde{\boldsymbol{\sigma}}$ is given by the following local constitutive relationship:

$$\tilde{\mathrm{s}}(\alpha, \beta) = (1 - \tilde{\omega}(\alpha, \beta)\mathbf{I}^{4s})\mathbf{C}_L^{-1} : \tilde{+}(\alpha, \beta) \tag{15}$$

where $\tilde{+}$ is the macrocrack local strain, $\tilde{\omega}$ is the macrocrack damage parameter. From the above, the inelastic strain of macrocracks can be written in terms of the local strain of macrocracks: $\hat{+}_i = (\mathbf{I}^{4s} - \tilde{\mathbf{M}}_{s_i}) : \tilde{+}_i$ where $\tilde{\mathbf{M}}_{s_i} = (1 - \tilde{\omega}_i)\mathbf{I}^{4s}$. The dependencies of $\tilde{\omega}$, including orientation, have been dropped for clarity.

The same damage surface (Eq. 9) employed for microcracks applies for calculating the effective strain parameter of macrocracks $\tilde{\zeta}$ and the evolution of the macrocrack damage parameter $\tilde{\omega}$ respectively.

Once the transition to localised damage has been initiated, inelastic strain $\hat{+}$ due to macrocracking starts to progress. But it is assumed that microcracks are still present in the band of material outside of the zone of localised cracking. Therefore, to capture the effect of macrocracking on microcrack growth, the inelastic macrocrack strain is removed from the local macrocrack strains:

$$+_L(\psi_k, \theta_k) = \mathbf{N}_{+}(\psi_k, \theta_k) : \left( \bar{+} - \sum_{isd=1}^{n_{sd}} \mathbf{N}_{\varepsilon}(\alpha_{isd}, \beta_{isd}) : \hat{+}(\alpha_{isd}, \beta_{isd}) \right) \tag{16}$$

A staggered solution is used to calculate the inelastic strain $\hat{+}$, the full details of which are presented in a forthcoming publication.

## 4 NUMERICAL SIMULATIONS

Uniaxial tension predictions from the two versions of the model (only microcracking and both microcrack and macrocrack growth) were compared to uniaxial tension lattice simulations of 10 random arrangements of aggregate particles. The intention of the comparisons is to show how a micromechanics based constitutive model for concrete which includes a crack localisation mechanism agrees well with more computationally expensive lattice simulations that discretely model the influence of the heterogeneous material structure of concrete at the meso-scale.

The material parameters employed in the constitutive model for these numerical simulations are given in Table 2. The lattice simulations were carried out using a 40% total volume fraction of aggregate particles and by maintaining the periodic cell and element, dimensions and material parameters described in Section 2

Table 2. Material parameters for the micromechanics based constitutive model.

| | |
|---|---|
| $E_m$(MPa) | 30 000 |
| $E_\Omega$(MPa) | 45 000 |
| $\nu_m$ | 0.19 |
| $\nu_\Omega$ | 0.21 |
| $\mathrm{f}_m$ | 0.6 |
| $\mathrm{f}_\Omega$ | 0.4 |
| $f_t$ (MPa) | 3 |
| $\varepsilon_0$ | 0.003 |

The numerical results are presented in Figure 4. When macrocrack localization is not included the response is overly ductile, whereas the inclusion of the transition to localized cracking leads to more realistic results and a better agreement with the lattice simulations. It can be observed in Figures 4b&c that in the micro-macro transition model, after the peak stress, damage becomes localised to a macrocrack plane and microcrack growth is stalled, much like what has been observed from the lattice experiments. In contrast, in the microcracking only model the microcrack planes continue to become damaged.

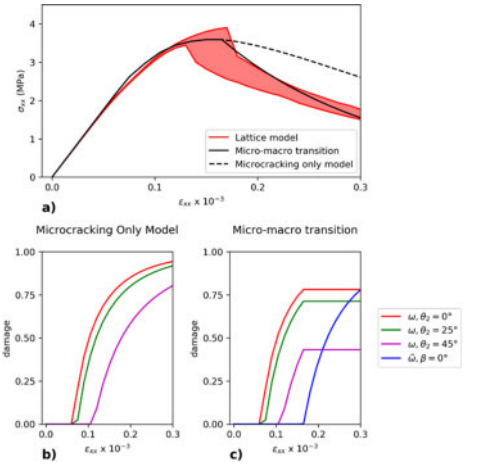


Figure 4. Uniaxial tension predictions. a) Stress-strain response. b) Damage evolution for the microcracking-only model. c) Damage evolution for the micro-macro transition model.

The proposed constitutive model captures well the characteristic behaviour of cementitious materials and associated cracking mechanisms, including the transition from diffuse microcracking to localized macrocracking.

## 5 CONCLUSIONS

A micromechanics based constitutive model for cementitious materials that addresses the transition from diffuse microcracking to localized macrocracking was presented. The good agreement between the proposed constitutive model and the lattice simulations demonstrated the potential of the constitutive model which captures well the characteristic mechanical behaviour of these materials and associated cracking mechanisms.

## REFERENCES


Budiansky, B. & O'Connell, R.J. 1976. Elastic moduli of a cracked solid. *International Journal of Solids and Structures*, 12: 81–97.

Grassl, P. & Antonelli, A., 2019. 3D network modelling of fracture processes in fibre-reinforced geomaterials. *International Journal of Solids and Structures,* Volume 156–157, 234–242.

Grassl, P. & Bolander, J., 2016. Three-dimensional network model for coupling of fracture and mass transport in quasi-brittle geomaterial. *Materials* 9(9): 782–800.

Jenq, Y-S. & Shah, S.P. 1991. Features of mechanics of quasi-brittle crack propagation in concrete. *International Journal of Fracture,* 51:103–120.

Karihaloo, B.L. 1995. *Fracture Mechanics and Structural Concrete.* Essex, England: Longman Scientific & Technical.

Mihai, I.C. & Jefferson, A.D. 2011. A numerical model foe cementitious composite materials with an exterior point Eshelby microcrack initiation criterion. *International Journal of Solids and Structures*, 48: 3312–3325.

Mura T. 1987. *Micromechanics of Defects in Solids. Second, revised edition*, Martinus Nijoff Publishers, The Netherlands.

Nemat-Nasser, S. & Hori, M. 1993. *Micromechanics: Overall Properties of Heterogeneous Materials*. Amsterdam: North-Holland.

Shah, S.P, Swartc, S.E. & C,O. 1995. *Fracture Mechanics of Concrete.* New York: John Wiley & Sons.

Slate, F.O. & Hover, K.C. 1984. Microcracking in concrete. In *Fracture Mechanics of Concrete:Material characterization and testing.* Dordrecht: Springer, 137–159.

Vonk, R.A. 1992. Softening of concrete loaded in compression. *PhD Thesis.* Eindhoven University of Thechnology, The Netherlands.